Light-Intensity and Thickness Dependent Efficiency of Planar Perovskite Solar Cells: Charge Recombination versus Extraction

Tian Du,[1,2] Weidong Xu,[2] Shengda Xu,[1] Sinclair Ratnasingham,[1,3] Chieh-Ting Lin,[1,2] Jinhyun Kim,[2] Joe Briscoe,[3] Martyn A. McLachlan[1]* and James R. Durrant[2,4,]*

[1]*Department of Materials and Center for Processable Electronics, Imperial College, London, W12 0BZ, United Kingdom*

[2]*Department of Chemistry and Center for Processable Electronics, Imperial College, London, W12 0BZ, United Kingdom*

[3]*School of Engineering and Materials Science, Queen Mary University of London, London, E1 4NS, United Kingdom*

[4]*SPECIFIC IKC, College of Engineering, Swansea University, SA2 7AX, United Kingdom*

Correspondence:

j.durrant@imperial.ac.uk

martyn.mclachlan@imperial.ac.uk

Supporting Information

Experimental Details

Device fabrication

All devices were fabricated on indium-doped tin oxide (ITO) coated glass substrates that were sequentially cleaned in acetone, isopropanol and deionized water (using ultrasonics) for 10 minutes followed by a N_2 dry. Prior to any deposition the substrates were treated by oxygen plasma for 10 minutes. PolyTPD (0.25wt. % in chlorobenzene) was spin-coated onto the ITO at 5000 rpm for 20s. After drying for 1 minute, PFN (0.05wt. % in methanol) was spin-coated onto the HTLs at 5000 rpm for 20s. All depositions were performed in ambient conditions prior to transfer to a N_2 filled glovebox.

The $CH_3NH_3PbI_3$ (MAPI) precursor solution was prepared by dissolving equimolar concentrations (1.5 M) of lead iodide (PbI_2, 99.985%, Alfa Aesar) and methylammonium iodide (MAI, Dyesol) in a mixed solvent of N,N-Dimethylmethanamide (DMF) and dimethyl sulfoxide (DMSO) (9:1.1 in volume ratio), and passed through a 0.45 µm PTFE filter before use. 40 µl precursor solution was dropped onto HTM coated substrate and spun at 4000 rpm for 30s. After 7 seconds, 0.5 ml diethyl ether (DE) was dripped onto the spinning substrate. The substrates were subsequently annealed on a hot plate at 100 °C for 15 minutes.

Solutions of the electron transport material were prepared by dissolving 23 mg/ml phenyl-C_{61}-butyricacid methylester (PCBM, Ossila) in chlorobenzene. The solution was stirred at 40 °C for 1h prior to use and filtered through a 0.45 µm PTFE filter before use. The PCBM solution was spin-coated on to MAPI films at 2000 rpm for 45 s. An ultra-thin interfacial dipole layer was deposited by spin-coating Bathocuproine (BCP) solution (0.5 mg/ml in methanol) on PCBM layer at 4000 rpm for 30 s. Finally, the devices were completed by thermally evaporating 100 nm of Ag at a base pressure of $5x10^{-6}$ mbar. The

device active area was 0.09 cm^2 (0.3 x 0.3 cm).

J-V measurement

Current density-voltage (J-V) characteristics were measured using a Keithley 2400 source meter. The cells were illuminated by an AM 1.5 filtered xenon lamp (Oriel Instruments) at 1 sun intensity, calibrated using a Si reference photodiode. All devices were stored in dark prior to measurement and were measured in a nitrogen-filled chamber. External quantum efficiency (EQE) spectra were measured with a PV Measurements QEX10 system. The spectral response was measured between 300 and 850 nm and was calibrated with a silicon reference photodiode.

Light intensity-dependent J-V curves were measured with an array of power-tunable white-light LEDs. The light intensity of LED was calibrated to 1-Sun equivalent according to the J_{SC} of solar cells measured under AM1.5 solar simulator, and was tuned by adjusting the power input. Weak-light performance of the solar cells was also measured with solar simulator with neutral density filter.

Physical and morphological characterization.

X-ray diffraction (XRD) patterns were obtained with a X'pert Powder diffractometer (PANalytical), Cu Kα source. The diffraction patterns were measured over the range 7 - 40° 2θ. The samples were rotated during measurement. The surface and cross-sectional scanning electron microscopy (SEM) images were obtained using a LEO Gemini 1525 field emission gun scanning electron microscopy. The working voltage of SEM was fixed at 5 kV. To prevent electrical charging, all films were coated with a thin chromium layer.

Photoluminescence and absorption spectroscopy measurements.

Photoluminescence spectroscopy of full devices were measured with a FL 1039 spectrometer (Horiba Scientific). Illumination was provided by a 635 nm continuous-wave laser adjusted to 0.2 Sun, 1 Sun and 6 Sun equivalent intensity by matching device current under both solar simulator illumination and laser illumination. Two short pass filters with edge of 700nm were used before samples to cut off the unwanted light after 700 nm and two long pass filters after 700 nm were used before the detectors to avoid white light background. The PL decay was measured by time-correlated single-photon counting with Horriba spectrofluorimeter with 404 nm excitation. Ultraviolet-visible (UV-Vis) absorption spectra were measured with a Horriba UV-vis spectrophotometer by measuring both transmittance and reflectance spectra of the perovskite films, with step-size of 1nm and integrating time of 0.5s.

Transfer-matrix optical modelling.

Both the normalised electric field distributions and the generation rate distribution were calculated using a Matlab script developed by Burkhard *et al*,[38] adopted from a transfer matrix method published by Peumans *et al*[53] and Pettersson *et al*.[54] The device J_{sc} was calculated using a Python script developed by Ball *et al*,[55] based on a transfer matrix method by Steve Byrnes (http://sjbyrnes.com/fresnel_manual.pdf). The optical constants of $CH_3NH_3PbI_3$, refractive index (*n*) and extinction coefficient (*k*) are adopted from the work by Phillips *et al*.[56] The optical constants for glass, ITO, HTM, PCBM and Ag electrode in the calculation are adopted from the work by Burkhard *et al* and Lin et al.[11]

Supporting figures

Tuning perovskite layer thickness

The thickness of perovskite layer was modulated by varying the concentration of precursor in the solution, while the mix of solvent remains constant. **Figure S1a** shows the correlation of film thickness versus concentration of $CH_3NH_3PbI_3$ (mol dm^{-1}) in precursor solution. The minimum solution concentration used was 0.8 mol dm^{-1}, below which there will be visible pinholes in the as-cast films. The maximum solution concentration is 2 mol dm^{-1} using our recipe. In **Figure S1b**, the photographs of perovskite films show that the film surface already becomes rough when 2 mol dm^{-1} solution is used, and the SEM images shows coarsened grains.

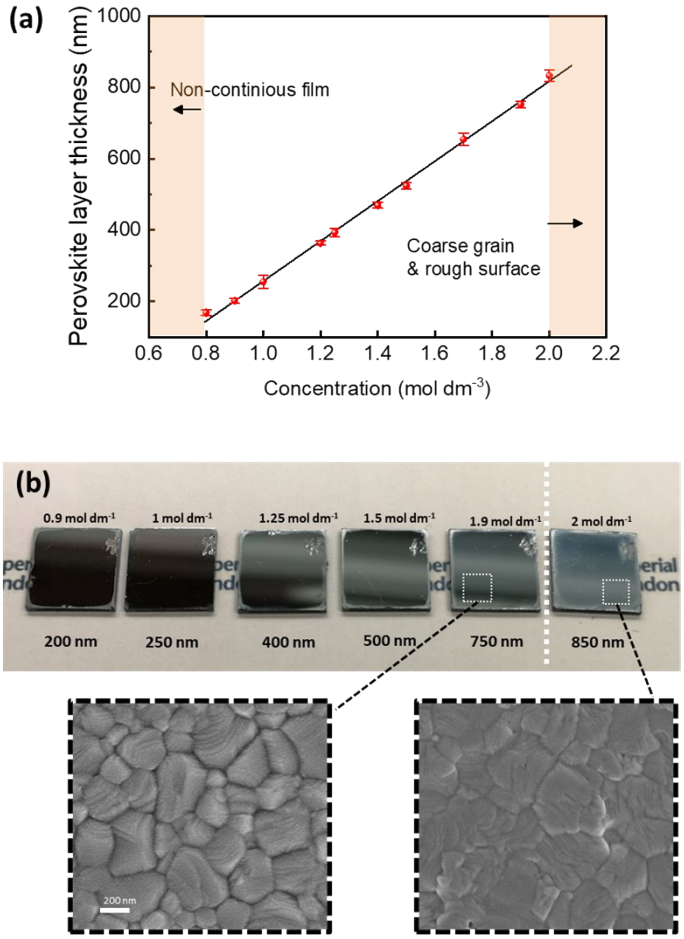

Figure S1. (a) Variation of $CH_3NH_3PbI_3$ perovskite film thickness with concentration of precursor solution containing PbI_2 and CH_3NH_3I of equal molar ratio. **(b)** Photographs of perovskite films prepared with precursor solution of different concentrations, and surface SEM images of perovskite films prepared with 1.9 mol dm^{-1} and 2 mol dm^{-1} solution.

Device performance under 1-Sun illumination

Figure S2 shows the J-V curves of perovskite solar cells (PSCs) with perovskite thickness ranging from 170 nm to 850 nm. **Figure S3** shows that J_{SC} no longer exhibits a sharp increase when thickness is above 200 nm. Instead, there is a clear continuous increase of V_{OC}. FF starts to drop radically as film thickness is greater than 750 nm due to interrupted film morphology.

Figure S4 Shows representative J-V characteristics at four representative light intensities. There is increased J-V hysteresis as light intensity is reduced, and the 250-nm devices exhibit the largest hysteresis.

Figure S5a shows the EQE spectra and integrated J_{SC} for the devices with different thickness, and **Figure S5b** the absorbance spectra of these perovskite films.

In Figure S2 there is moderate increase of J-V hysteresis as perovskite thickness is increased under 1 Sun. However, the stabilized PCE, **Figure S5 c - d**, measured by applying voltage near the maximum power point (mpp) is close to the PCE measured with reverse scanning. Thus we use the data from reverse-scanning protocol for device PCE comparison. **Figure S5** shows dark current density of 250 nm and 750 nm device.

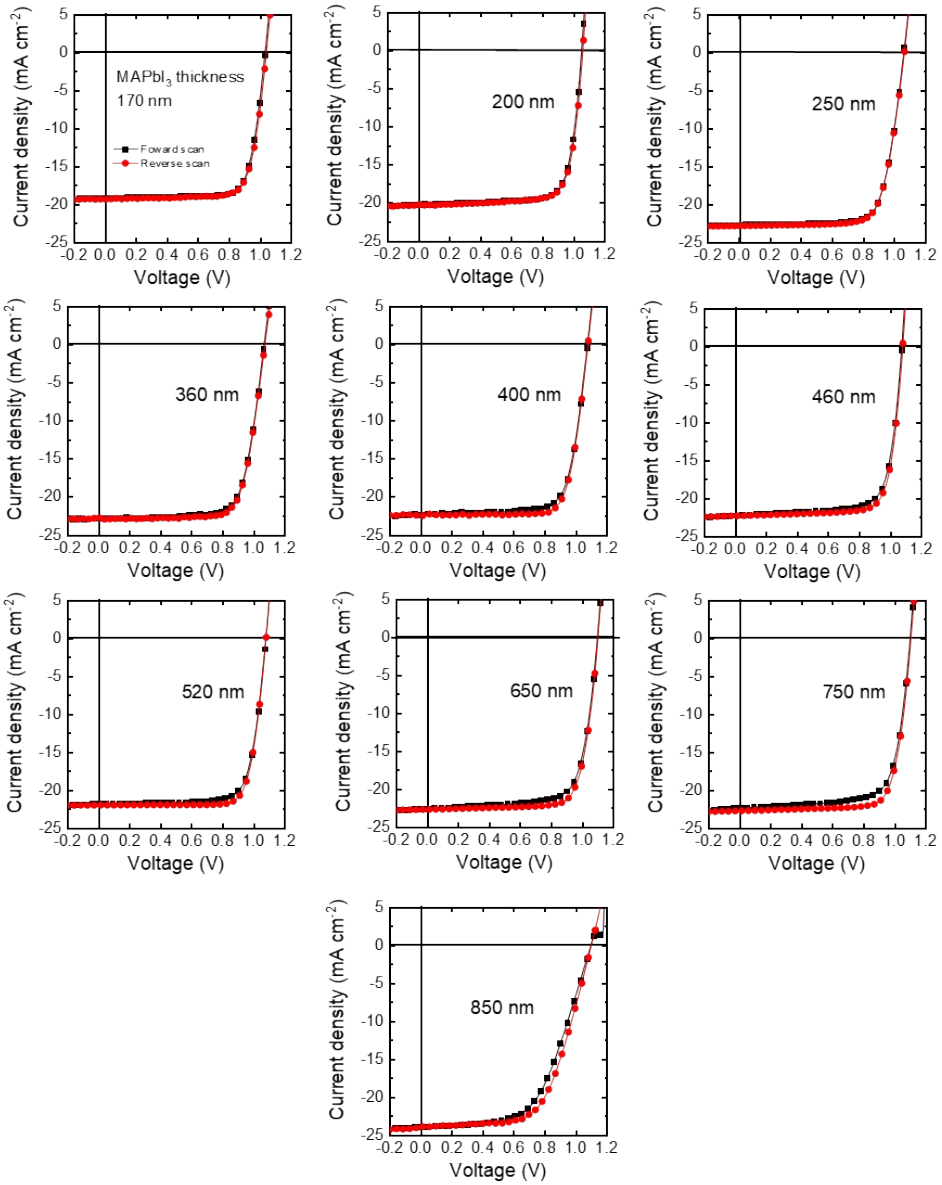

Figure S2. J-V characteristics of PSCs with varied perovskite thickness, measured under AM1.5 1-Sun equivalent illumination provided by a solar simulator. The scan rate is 50 mV s^{-1} for all devices, in both forward (-0.2 V – 1.2 V) and reverse (1.2 V – -0.2 V) direction.

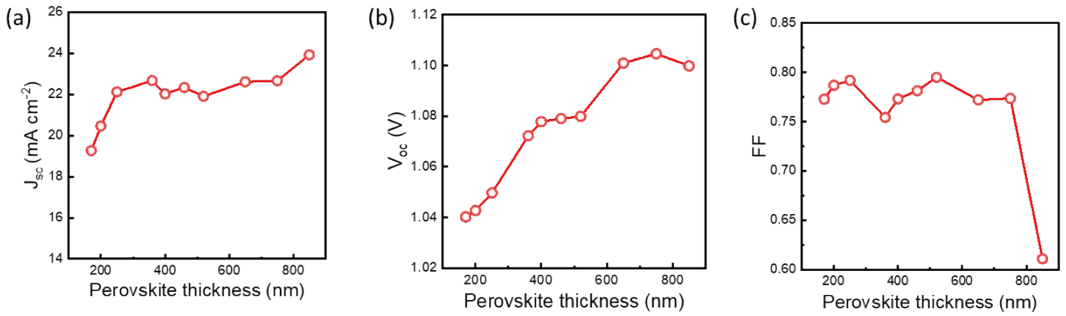

Figure S3. Photovoltaic parameters measured under 1-Sun illumination for devices with varied perovskite thickness, obtained from reverse scanning direction.

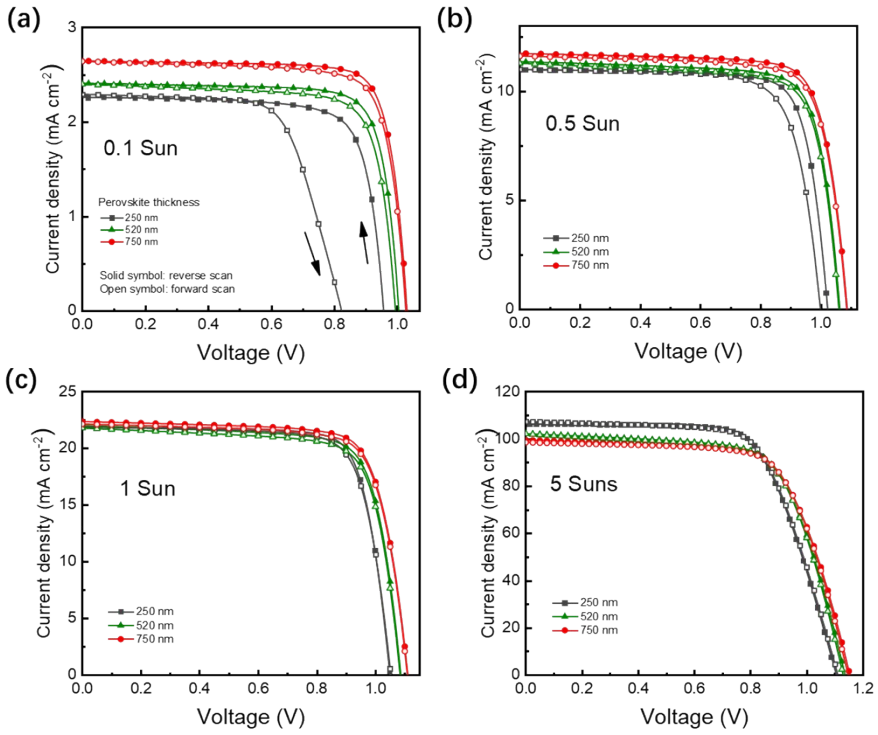

Figure S4. Representative J-V curves of 250, 500 and 750 nm thick active layer devices under light intensity of 0.1 Sun, 0.5 Sun, 1 Sun and 5 Suns, measured with both forward and reverse scanning direction at a rate of 50 mV/s.

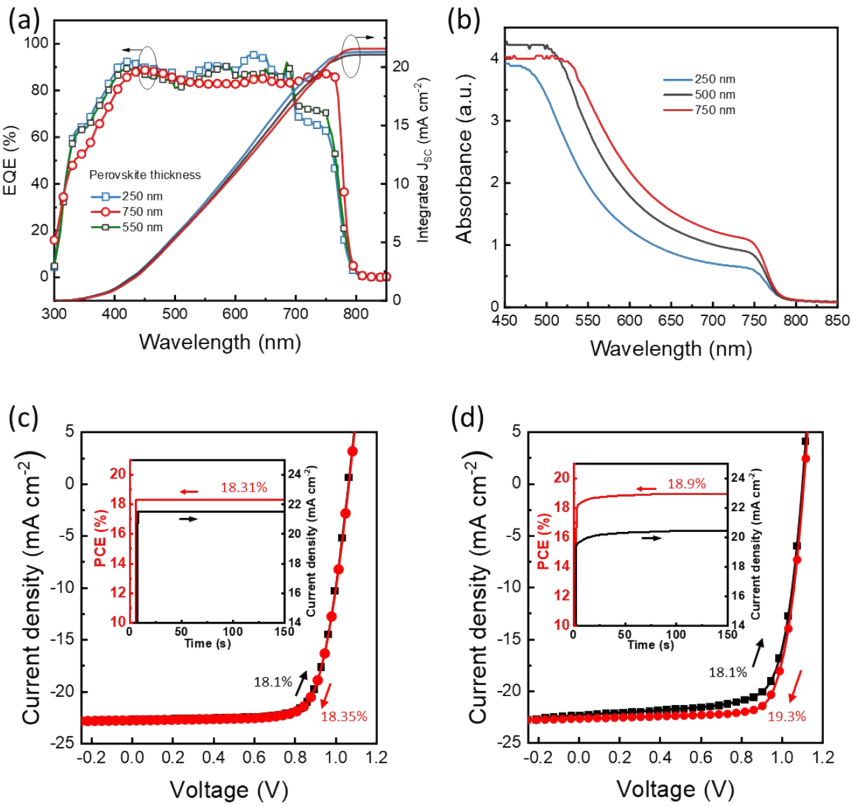

Figure S5. (a) External quantum efficiency (EQE) spectra of p-i-n PSCs. **(b)** UV-vis absorbance spectra of perovskite film of different thickness. **(c), (d)** Stabilized power conversion efficiency of the p-i-n PSCs with 250 nm and 750 nm perovskite layer, by holding the device at a voltage close to the maximum power point (MPP).

Structural characterization

The X-ray diffraction (XRD) data shows minimal change in the crystal structure of perovskite as thickness is altered. Analysis of the peak parameters shows negligible shift both in peak position that suggests minimal change in lattice parameter, and in full width at half maximum (FWHM) indicating a limited variation of crystallite size (< 20 nm), consistent with the SEM images. The peak intensity of (110) increases linearly with perovskite thickness, which is anticipated as the volume of materials that diffract x-ray scales with film thickness. However, there is a decrease of film orientation manifest by reduced ration of (110) peak intensity over (211) intensity, this is anticipated as multiple grains appears in the vertical direction as thickness increases. Interestingly, the reduction of film orientation is contrast to improvement of device performance, suggesting that performance enhancement enabled by increased perovskite thickness is not ascribed to change of film quality, but is due to suppression of interfacial recombination as is analyzed in the main text.

Table S1. Parameters of X-ray diffraction patterns of 250 nm and 750 nm perovskite films.

Perovskite film thickness /nm	(110) peak position /degree	(110) peak intensity /count	Crystallite size /nm	(110)/(211) relative intensity
250	14.16	9338.5	118	10.9
500	14.16	10682.2	106	8.5
750	14.15	11971.4	106	6.4

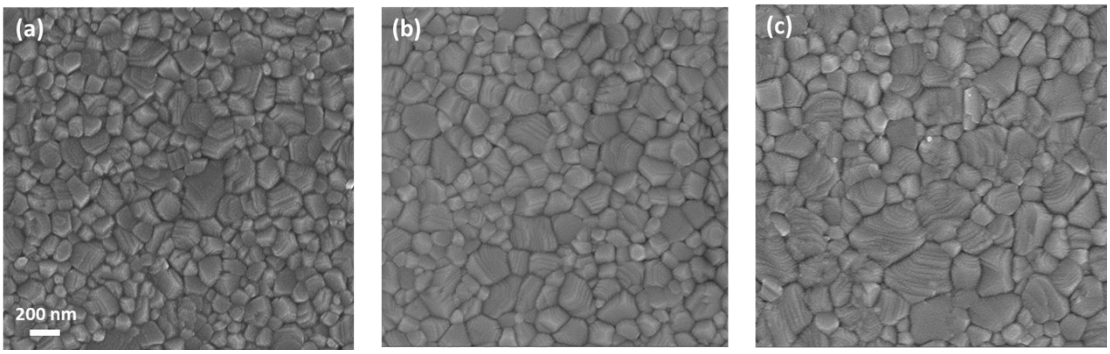

Figure S6. Top-view SEM images of perovskite films of (a) 250 nm, (b) 500 nm and (c) 750 nm.

Transfer-matrix optical modelling

Table S2 shows the source of parameters used in our optical modelling. Our modelling result indicate that the difference of J_{SC} is mainly caused by loss of reflection (Table S3). The ratio of reflection loss is constant under different light intensities, thus calculated J_{SC} shows rigid linearity with light intensity for all devices.

Table S2 Parameters of transfer optical modeling: thickness of each layer and the literature where optical constant of each layer is derived from.

Material	Glass	ITO	PTPD	MAPI	PCBM	Ag
Thickness (nm)	1000	110	10	250, 500, 750	40	100
Optical constant	Ball *et al*	Burkhard *et al*	Ball *et al*	Phillips *et al*	Burkhard *et al*	Ball *et al*

Table S3 Ratio of J_{SC} loss caused by reflection (1 Sun).

Perovskite thickness (nm)	Loss from reflection
250	22.1%
750	11.7%

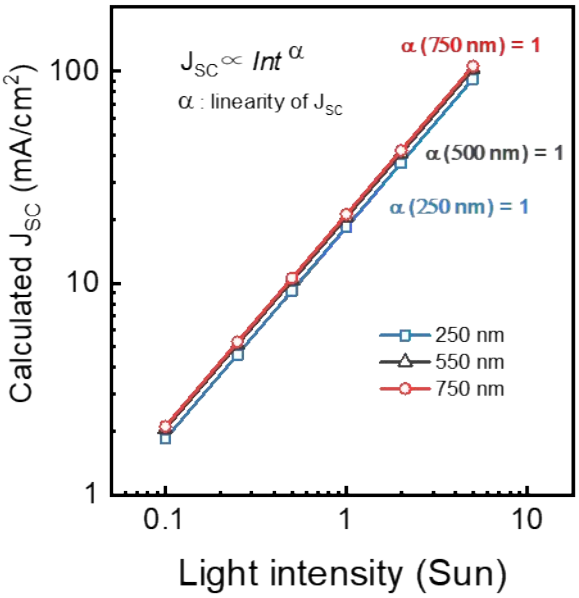

Figure S7. The calculated J_{SC} as a function of light intensity of p-i-n devices with perovskite layer of three different thickness.

Transient optoelectronic measurement

Transient photocurrent (TPC) and transient photovoltage (TPV) measurements were carried to probe the density of the lifetime of photo-excited charge at open circuit. TPV is a small perturbation technique, which is, the induced change in voltage by an optical perturbation is much smaller the background value ($\Delta V << V_{OC}$). TPV measurement is performed by ensuring open circuit condition, holding the device at different V_{OC} with power-tunable background illumination. As the device stabilizes at V_{OC}, the optical perturbation generates small number of additional charge, ΔQ, resulting in a small increase in quasi-fermi level splitting probed as ΔV. At open circuit condition the excess charge is forced to recombine and lifetime is probed by fitting the decay of photovoltage transient. The decay of TPV transients is proportional the decay of excess charge density provided small perturbation condition is maintained.

Figure S8 shows the differential capacitance calculated by $C_{DC}=\Delta Q/\Delta V$, where ΔV is obtained from TPV measurement and ΔQ is assumed to be determined by optical perturbation and is measured from TPC. Differential capacitance corresponds to the local gradient of the density of states. Integration of C_{DC} with respect to voltage yield the total charge in device at given V_{OC}. **Figure S9** shows that n follows an exponential energetic dependence V_{OC}: $n = n_0 exp(\frac{qV_{OC}}{mkT})$

the parameter *m* is related to the energetic disorder of the semiconductor and for idea semiconductor m=2. Herein the device with perovskite layer of 250 nm exhibits a rather high m of 6.8, and the 750-nm shows much smaller *m* of 3.1.

Figure S10 highlights that the small-perturbation lifetime decreases exponentially with V_{OC}

$\tau_{\Delta n} = \tau_{\Delta n,0} exp(\frac{qV_{OC}}{\vartheta kT})$

The parameter θ is slope of $\tau_{\Delta n}$-V_{OC}. Importantly, TPV only measures lifetime of the excess charge generated by optical perturbation. Although this lifetime is related to device performance as well, the total charge lifetime τ_n is most interesting for understanding. The small perturbation lifetime can be converted to total charge lifetime if the recombination order δ[7] $\tau_n = \delta\tau_{\Delta n}$

Table S5 shows that the reaction order of 250-nm is much higher than 2, indicative of high-order recombination processes. However, as ref [7] pointed out this is more likely owing to spatially inhomogeneous distribution of charge. The 750-nm device, on the contrary, exhibit a reaction order close to 2, consistent with its improved homogeneity in charge distribution.

If we have correctly estimated the amount excess charge accumulated in the working device (*n*), and the measured photovoltage decay time-constants (τ) are related to a recombination process then we should be able to calculate device V_{oc} using only these measured data and their corresponding fitting parameters. At open circuit the recombination flux will equal the flux of

generated charge, J_{rec} = J_{gen}. J_{rec} is described with the measured charge density n and the total recombination lifetime τ_n for this quantity of charge:

$$J_{rec} = -\frac{qn}{\tau_n}$$

J_{gen} can be estimated by the short circuit current density J_{sc} at each light intensity, shown in **Figure S11**. The reconstructed open circuit voltage, V_{oc}^{Rec}, can be found by

$$V_{oc}^{Rec} = \frac{mk_BT}{q\delta}\ln\left(\frac{\tau_{n,0}J_{SC}}{qn_0}\right).$$

and is plot versus measured V_{OC} in **Figure S12**.

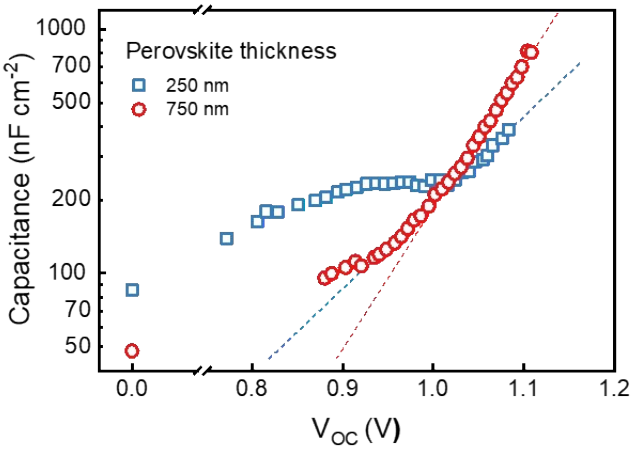

Figure S8. Difference capacitance of p-i-n solar cells with perovskite layer of three different thickness.

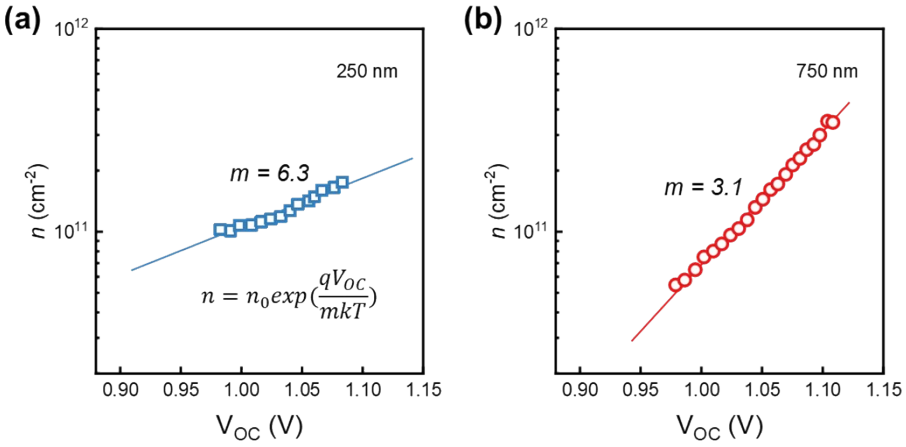

Figure S9. Fitting of n [cm^{-2}] versus V_{OC}.

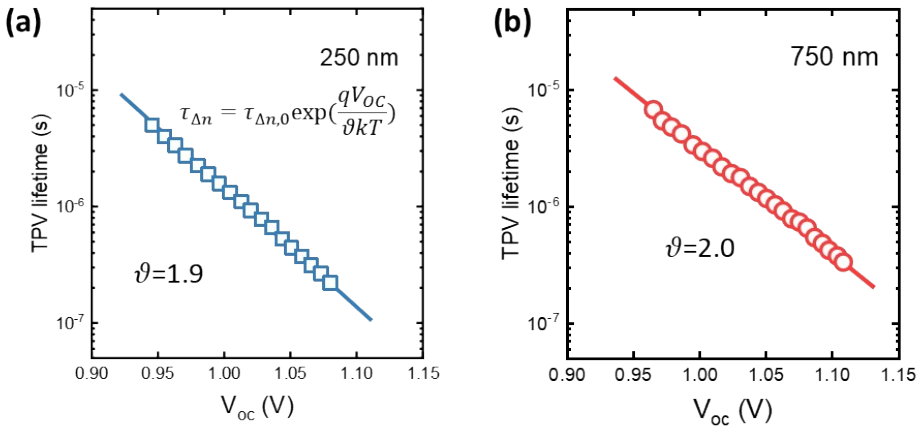

Figure S10. Fitting of TPV lifetime $\tau_{\Delta n}$ versus V_{OC}.

Table S4 Fitting parameters in transient optoelectronic measurements.

Perovskite thickness	m	ϑ	$\boldsymbol{\delta}$	$\tau_{n,0}$ (ns)	n_0 (cm^{-2})
250 nm	6.3	1.9	**5.2**	4500	1.5×10^{7}
750 nm	3.1	2.0	**2.6**	1100	3.3×10^{3}

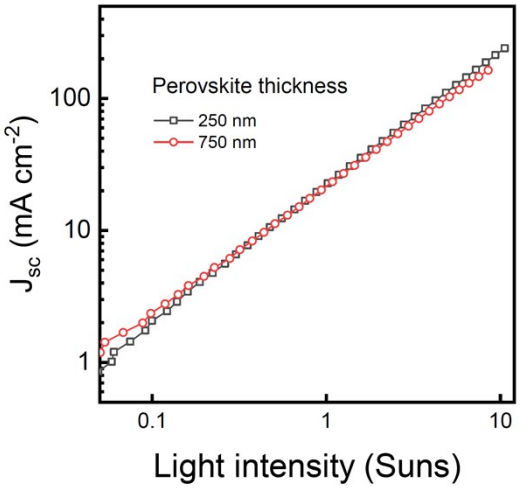

Figure S11. Measured J_{SC} as a function of light intensity within the same range of V_{OC}-Light measurement.

Reference

1 G. F. Burkhard, E. T. Hoke and M. D. McGehee, *Adv. Mater.*, 2010, **22**, 3293–3297.

2 P. Peumans, A. Yakimov and S. R. Forrest, *J. Appl. Phys.*, 2003, **93**, 3693–3723.

3 L. A. A. Pettersson, L. S. Roman and O. Inganäs, *J. Appl. Phys.*, 1999, **86**, 487–496.

4 J. M. Ball, S. D. Stranks, M. T. Hörantner, S. Hüttner, W. Zhang, E. J. W. Crossland, I. Ramirez, M. Riede, M. B. Johnston, R. H. Friend and H. J. Snaith, *Energy Environ. Sci.*, 2015, **8**, 602–609.

5 L. J. Phillips, A. M. Rashed, R. E. Treharne, J. Kay, P. Yates, I. Z. Mitrovic, A. Weerakkody, S. Hall and K. Durose, *Sol. Energy Mater. Sol. Cells*, 2016, **147**, 327–333.

6 Q. Lin, A. Armin, R. Chandra, R. Nagiri, P. L. Burn and P. Meredith, *Nat. Photonics*, 2014, **9**, 106–112.

7 T. Kirchartz and J. Nelson, *Phys. Rev. B - Condens. Matter Mater. Phys.*, 2012, **86**, 1–12.